Journal of Geodynamics 121 (2018) 143–154

Contents lists available at ScienceDirect

Journal of Geodynamics

journal homepage: www.elsevier.com/locate/jog

Estimation of optimum velocity model and precise earthquake locations in NE Aegean: Implications for seismotectonics and seismic hazard

K.I. Konstantinou

Dept of Earth Sciences, National Central University, Jhongli, 320 Taiwan

ARTICLE INFO

Keywords:
Aegean
Greece
Seismicity
Relocation
Seismic hazard

ABSTRACT

This study relocates the seismicity in NE Aegean during the period 2011–2017 using data recorded by the Hellenic Unified Seismic Network (HUSN) in order to elucidate the relationship between seismicity and active faults in this area. P- and S-phase travel times of well-recorded events were first inverted in order to derive a minimum 1D velocity model with station delays using VELEST. Absolute locations of 4450 events were obtained by use of the nonlinear probabilistic algorithm NLLOC and the newly derived velocity model. Precise relative locations with horizontal and vertical uncertainties that do not exceed 1.2 km were calculated for 3354 events using the double-difference algorithm. The relocated seismicity delineates active faults to the south of Lesvos island, at the tip of Biga peninsula in Turkey and along the parallel strands of strike-slip faults that accommodate the westward motion of Anatolia. The comparison of the seismicity distribution with known active faults and the regional stress field shows that the strike-slip faults represent either principal shear zones, or Riedel shears oriented obliquely to the minimum stress axes. Normal faults are oriented almost perpendicular to the direction of the minimum stress axes in accordance with the transtensional deformation model. The seismogenic layer thickness derived from the depth distribution of relocated seismicity was found to be in the range of 14.8–15.8 km. By combining this thickness with geometrical characteristics of active faults and with a relationship that connects moment magnitude with rupture area, it is possible to estimate expected magnitudes of earthquakes. These magnitudes range from 6.3 to 7.2 depending on the rupture scenario that is considered for each fault. Of particular concern are the faults of Agia Paraskevi in Lesvos and Mastichochoria in Chios island that traverse densely populated areas and can produce large events with magnitudes from 6.4 to 6.9. Very little seismicity can be observed along these faults in the past 7 years, which may indicate either that they are creeping, or that they are locked and accumulate strain energy.

1. Introduction

The Aegean is an area of intense deformation as a result of the gravitational spreading of the Aegean lithosphere and the westward motion of Anatolia (Hatzfeld et al., 1997; Meijer and Wortel, 1997; Nyst and Thatcher, 2004; Hollenstein et al., 2008; Floyd et al., 2010; Konstantinou et al., 2016). In the northern part of the area, the North Aegean Trough forms a series of pull-apart sedimentary basins bounded by NE-SW strike-slip faults that represent the different branches of the North Anatolian Fault in the Aegean (Papanikolaou et al., 2002; Koukouvelas and Aydin, 2002; McNeill et al., 2004; Beniest et al., 2016) (Fig. 1). To the south of the North Aegean Trough from the Turkish coast up to the island of Skyros, several other branches with the same orientation can be observed that delineate smaller pull-apart basins. While the kinematics of these faults exhibit dextral sense of motion, they are interrupted by NW-SE oriented sinistral strike-slip faults such as the ones to the north of Skyros island (cf. Fig. 1). These faults are thought to be older structures that became reactivated with a sinistral sense of motion under the present-day stress field (Kiratzi, 2002). GPS observations confirm the notion that the faults bounding the North Aegean Trough accommodate most of the westward motion of Anatolia and that the faults to the south of it are less developed, as indicated by their smaller strain and slip rates (Kreemer et al., 2004; Müller et al., 2013).

Seismicity in the NE Aegean is quite high as suggested by several large (Mw > 6.0) earthquakes that have occurred during the last 73 years (Papazachos and Papazachou, 2003) (cf. Fig. 1 and Table 1). The majority of them have nucleated along the NE-SW oriented strike-slip faults, even though there are notable exceptions to this trend. The first of these exceptions is the 2001 Skyros (Mw ~6.4) earthquake that ruptured one of the older NW-SE oriented strike-slip faults (Karakostas et al., 2003; Roumelioti et al., 2003). The second exception has to do

E-mail address: kkonst@cc.ncu.edu.tw.

https://doi.org/10.1016/j.jog.2018.07.005
Received 28 February 2018; Received in revised form 21 June 2018; Accepted 26 July 2018
Available online 11 September 2018

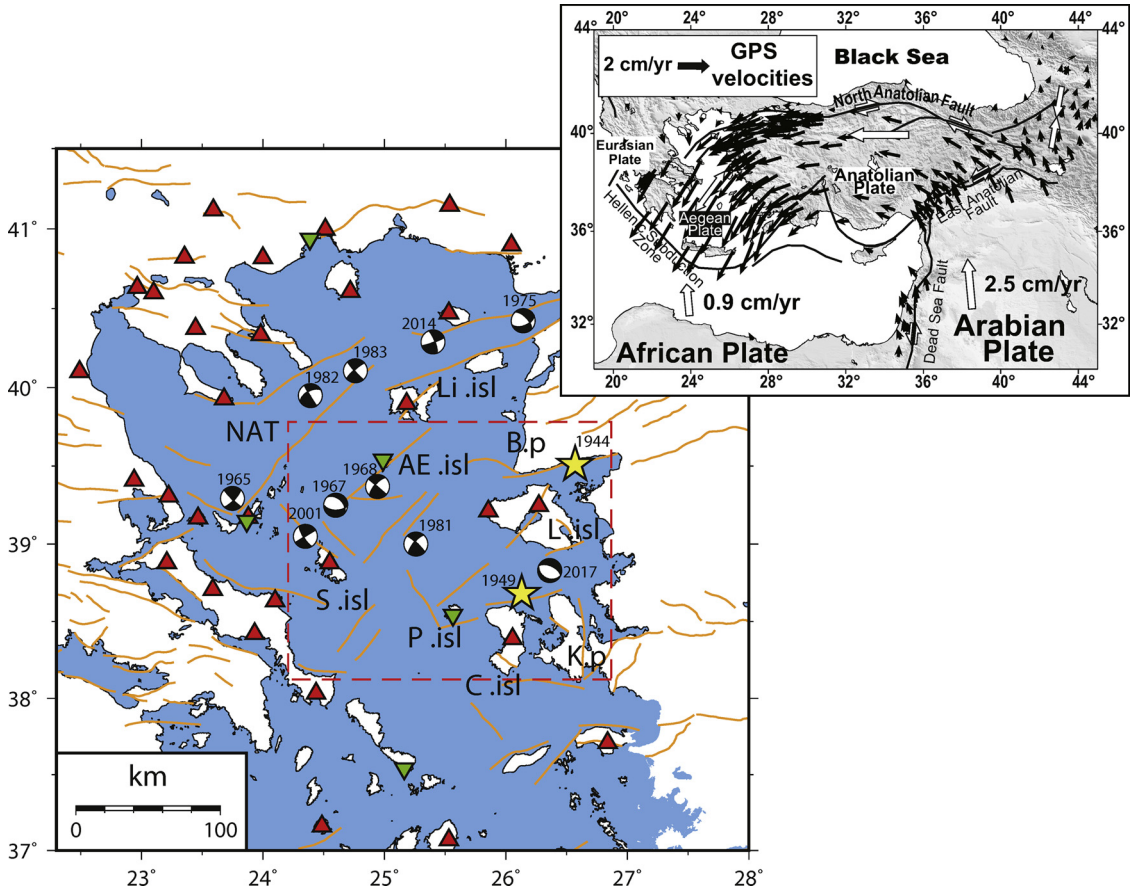

Fig. 1. Map showing the area of northern and central Aegean. The red dashed line outlines the study area. Solid orange lines represent active faults contained in the GReDaSS database (Caputo and Pavlides, 2013). The two yellow stars represent the 1944 Edremit and 1949 Chios-Cesme earthquakes, while focal mechanism solutions of other large (> 6) earthquakes that have occurred in the area are also shown as black beach balls (see Table 1 and text for more details). Red triangles represent HUSN weak-motion stations and green inverted triangles represent the strong-motion stations. The inset at the upper right hand corner depicts the geodynamic setting in the eastern Mediterranean and the GPS velocity field (after Reilinger et al., 2010). NAT: North Aegean Trough, Li.isl: Limnos island, AE.isl: Agios Efstratios island, S.isl: Skyros island, B.p: Biga peninsula, L.isl: Lesvos island, K.p: Karaburun peninsula, C.isl: Chios island, P.isl: Psara island. (For interpretation of the references to colour in this figure legend, the reader is referred to the web version of this article).

Table 1
List of source parameters for large earthquakes (Mw > 6) that have occurred within the study area during the last 73 years. The ISC-GEM global catalog (Storchak et al., 2013) is used for events prior to the existence of HUSN. Date is in year, month, day format, OT is origin time in hour, minutes, seconds format and H signifies hypocentral depth. The focal mechanisms of these events are shown in Fig. 1.

Date	OT	Lat (°N)	Lon (°E)	H (km)	Mw	Reference
19441006	02:34:47	39.509	26.587	15	6.7	ISC-GEM
19490723	15:03:35	38.718	26.482	15	6.5	ISC-GEM
19670304	17:58:06	39.1	24.684	15	6.6	ISC-GEM
19680219	22:45:45	39.368	24.957	15	7.2	ISC-GEM
19811219	14:10:54	39.259	25.294	14	6.8	ISC-GEM
20010726	00:21:39	39.051	24.258	15	6.4	ISC-GEM
20170612	12:28:38	38.839	26.369	11	6.3	NOA

with earthquakes that nucleated along normal rather than strike-slip faults (e.g. the 1967 Mw 6.6 Skyros earthquake), implying a rather complex seismotectonic regime for the NE and central Aegean. More recently this area experienced further seismic unrest, first during January-March 2017 when a swarm consisting of hundreds of events occurred at Biga peninsula, and then in June 2017 when a major earthquake (Mw ~6.3) struck near the south coast of Lesvos island. The fact that most of these faults lie beneath the sea surface means that in situ observations are inadequate for resolving their characteristics. Seismological observations can be used instead in order to understand fault geometry and kinematics; however, for such an approach to be fruitful precise earthquake locations are needed that can delineate the faults both at shallow and deeper levels within the crust.

This work relocates the seismicity in NE Aegean motivated primarily by the need to understand the geometry and segmentation characteristics of active faults and to estimate the thickness of the seismogenic layer, all of which can help towards assessing seismic hazard in the area. First, a brief summary of the available data is given in terms of network configuration and routine data processing. A minimum 1D velocity model with station delays for P- and S-waves is then derived by inverting travel times of well-recorded events. Improved absolute and precise relative locations are calculated by using the newly derived optimum velocity model in an effort to accurately delineate the seismogenic sources that lie within the study area and correlate them to known active faults. Finally, the discussion focuses on the relationship of these seismogenic sources with the regional stress field and their potential to nucleate large earthquakes in the future.

2. Data

The Hellenic Unified Seismic Network (hereafter called HUSN) represents the permanent seismic network that monitors earthquake activity in the Aegean as well as in mainland Greece. HUSN is the result of the merging in 2008 of three networks operated by Greek universities (Athens, Thessaloniki and Patras) with the nationwide network

operated by the National Observatory of Athens (hereafter called NOA), Institute of Geodynamics. All HUSN stations are equipped with three-component sensors that are broadband up to 20–120 s depending on the sensor type (CMG-40 T, CMG-3ESP, Lennartz Le-3D, STS-1, STS-2, Trillium 120 P). The recorded waveforms are then relayed in real time to NOA headquarters where events are routinely located by NOA staff after phase picking and assignment of quality weights to each pick. The NOA catalog was searched from January 2011 until December 2017 in order to find events within an area that covers the western Turkish coast up to the Greek island of Skyros (cf. Fig. 1). The use of data recorded during the period 2011–2017 has two main advantages: first, during this period HUSN exhibits the best quality and largest quantity of recordings since its initiation; and second, this period includes intense seismic activity that can give important hints in relation to the regional tectonics. The search yielded a total of 4,450 events that were recorded by 8 or more stations. Most of these events had local magnitudes smaller than 3.0, essentially representing microseismicity, six of them had local magnitude between 5.0–5.5, and the 12 June 2017 Lesvos earthquake was the largest event during this period. The study area is surrounded by 30 HUSN stations that offer good azimuthal coverage as can be seen in Fig. 1. An additional number of 5 strong-motion sensors whose phase picks can also be used, increases the available stations to 35 and fills some of the remaining azimuthal gaps.

3. Minimum 1D velocity model

A minimum 1D velocity model can be defined as the velocity model that produces the smallest possible uniform error for a set of events with well-constrained locations (Kissling et al., 1994). The software package VELEST (Kissling, 1995) estimates such a model by simultaneously inverting P- and S-wave travel times for a 1D velocity model, hypocentral locations and station delays. VELEST first solves the forward problem by tracing direct, reflected and refracted rays from source to receiver, and standard damped least squares is used in order to solve the inverse problem. For the purpose of applying this methodology to the dataset from NE Aegean, suitable events have to be selected that conform to the following criteria: (a) the number of P- and S-phases should be more than 15, (b) the azimuthal gap should be less than 180°, and (c) the RMS residual value should be less than 0.4 s. A total of 418 events were found to be in accordance with these criteria, yielding 5585 P-phases and 2446 S-phases. Station LIA (25.1805°, 39.89702°), placed on molasse deposits, was selected as the reference station since it recorded one of the largest number of phases and it is located near the center of the network. VELEST does not automatically adjust the thickness of the model layers after each iteration, therefore the initial model was parameterized with thickness equal to 2 km for the layers at the top 20 km and 5 km for the layers deeper than that.

As with all inverse problems, obtaining a minimum 1D velocity model relies on finding a robust minimum in the solution space rather than a local one. In order to explore as much as possible the model space, a series of 60 initial models were constructed whose velocities were subjected to the constraint not to contain low velocity layers. At first, only P-wave travel times were inverted for the reason that P-phases provide better spatial sampling and involve smaller picking errors. Fig. 2 shows the 60 initial models and also the 12 final models that exhibited the lowest RMS residual (~0.29 s). It can be seen that these models become very similar in the depth interval 5–20 km, while they display more variation at 20–35 km and at the top 5 km. This variation can be easily explained by considering that ray density significantly decreases below 20 km, which results in unconstrained velocities for these depths, and that rays at the top 5 km are almost vertical and thus do not sample the medium adequately. The final P-wave velocity model is then taken as the average of these 12 models and subsequently S-phase travel times were also inverted in order to derive the minimum 1D S velocity model. The final P and S velocity models as well as the variation of the Vp/Vs ratio as a function of depth can be seen in Fig. 3.

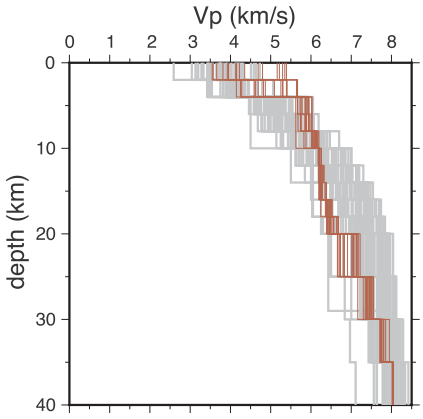

Fig. 2. P-wave velocities versus depth for the 60 initial models (grey lines) that were used as input to VELEST and 12 final models (red lines) that exhibited the smallest RMS residual. (For interpretation of the references to colour in this figure legend, the reader is referred to the web version of this article).

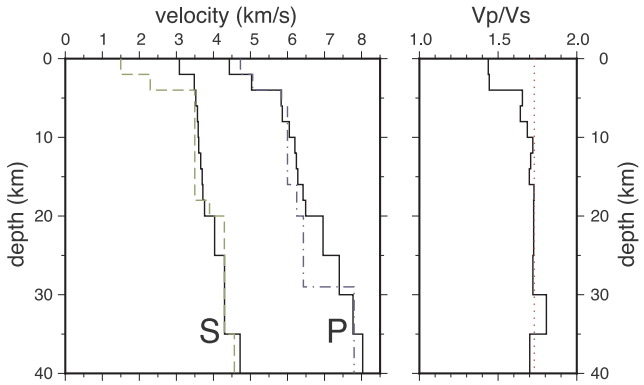

Fig. 3. Final P and S velocity models along with the corresponding Vp/Vs ratio (black lines) as a function of depth. The blue dash-dotted line corresponds to the P velocity model for western Anatolia derived by Akyol et al. (2006). The green dashed line represents the shear wave variation as a function of depth derived for NE Aegean from Rayleigh wave dispersion by Karagianni et al. (2005). The red dotted line indicates the Vp/Vs ratio value of 1.73. (For interpretation of the references to colour in this figure legend, the reader is referred to the web version of this article).

A comparison of the P velocity model with the velocity model derived by Akyol et al. (2006) for western Anatolia shows a good agreement, with the model derived in this study being 4%–5% faster in the interval 10–20 km. These faster velocities may indicate that the crust in the NE Aegean is cooler, less fractured and/or more dry than the crust in the adjacent area of western Anatolia. Similarly, the S velocity model agrees relatively well with the shear wave velocity profile obtained from inversion of Rayleigh waves in NE Aegean (Karagianni et al., 2005).

One way to evaluate the robustness of the newly derived minimum 1D model is to randomly shift by some amount the initial hypocentral coordinates of the events before the inversion. If the proposed model is indeed a robust minimum in the solution space, the events will be relocated back to their previous positions and no significant changes in velocity will occur. This test was performed by perturbing the location coordinates of the input events by ± 7 km and then use VELEST to invert for event locations and P, S velocity model. It was found that the average difference between the original and recalculated locations was 20 m (± 200 m) in latitude, 250 m (± 430 m) in longitude and 1.3 km (± 1.2 km) in depth. The recalculated P, S velocity model is very close to the original, except from the top 5 km (Fig. 4). Another test that can be used to infer the reliability of the proposed model is to examine whether the station delays are in accordance with the near-

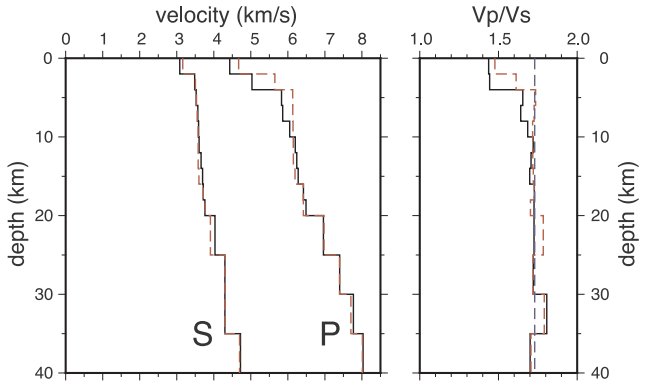

Fig. 4. Final P, S velocity model and Vp/Vs ratio (black lines) compared to the model obtained by using shifted earthquake locations (red dashed lines). The blue dashed line indicates the Vp/Vs ratio value of 1.73. (For interpretation of the references to colour in this figure legend, the reader is referred to the web version of this article).

surface geology at each station site. The stations included in this study are placed on three kinds of sites, namely soft rock (shists, tuffs), hard rock (limestone, marble, granite, lavas) and alluvium deposits. It can be seen that stations placed on hard rock exhibit negative delays (especially for P-waves), while stations placed on soft rock or alluvium deposits have almost zero or positive delays (Fig. 5). This means that the inverted delays correctly identify stations whose site exhibit higher true velocities (i.e. negative values) or lower true velocities (i.e. positive values) than the minimum 1D model.

4. Absolute locations

Using the newly derived minimum 1D model with station delays it is possible to estimate improved absolute locations for the events within the study area. Rather than utilizing linear approximations for solving the earthquake location problem, the freely available software package NLLOC (Lomax et al., 2000, 2009) is used instead. NLLOC employs a nonlinear probabilistic algorithm that calculates earthquake locations after reconstructing the posterior probability density function (PDF) (e.g. Tarantola and Valette, 1982; Moser et al., 1992) through the sampling of the solution space using the Oct-tree search algorithm (Lomax and Curtis, 2001). The maximum likelihood point of the complete posterior PDF is then considered to be the sought earthquake location. NLLOC also offers the option of using the Equal Differential-Time (EDT) function (Font et al., 2004) as the likelihood function to be maximized, which is formed from the differences of residuals recorded at pairs of stations. The advantage of combining the PDF formulation along with the EDT likelihood function is the ability of estimating robust locations even if the observed travel times contain large outliers.

A 3D grid consisting of 500 × 500 × 180 cells with node spacing of 1 × 1 × 1 km was employed in order to pre-calculate theoretical travel times for each station using the finite differences algorithm of Podvin and Lecomte (1991). Location uncertainties in the horizontal and vertical directions were calculated by using the diagonal elements of the covariance matrix (see Maleki et al., 2013). These elements are sensitive to the shape of the PDF and become large when this shape starts deviating from quasi-ellipsoidal, signifying a decrease in the location accuracy. Fig. 6 shows the locations of all events in the study area obtained with NLLOC by using the P and S minimum 1D model with station delays. Significant seismicity can be observed along the south coast of Lesvos island, partly due to the strong earthquake in June 2017, extending towards the Karaburun peninsula. A large number of events seems to be concentrated along the northern coast of Chios island and smaller clusters appear to the north and south of the island of Psara. North of Lesvos, at the tip of the Biga peninsula, a large cluster consisting of hundreds of events represents the swarm activity that

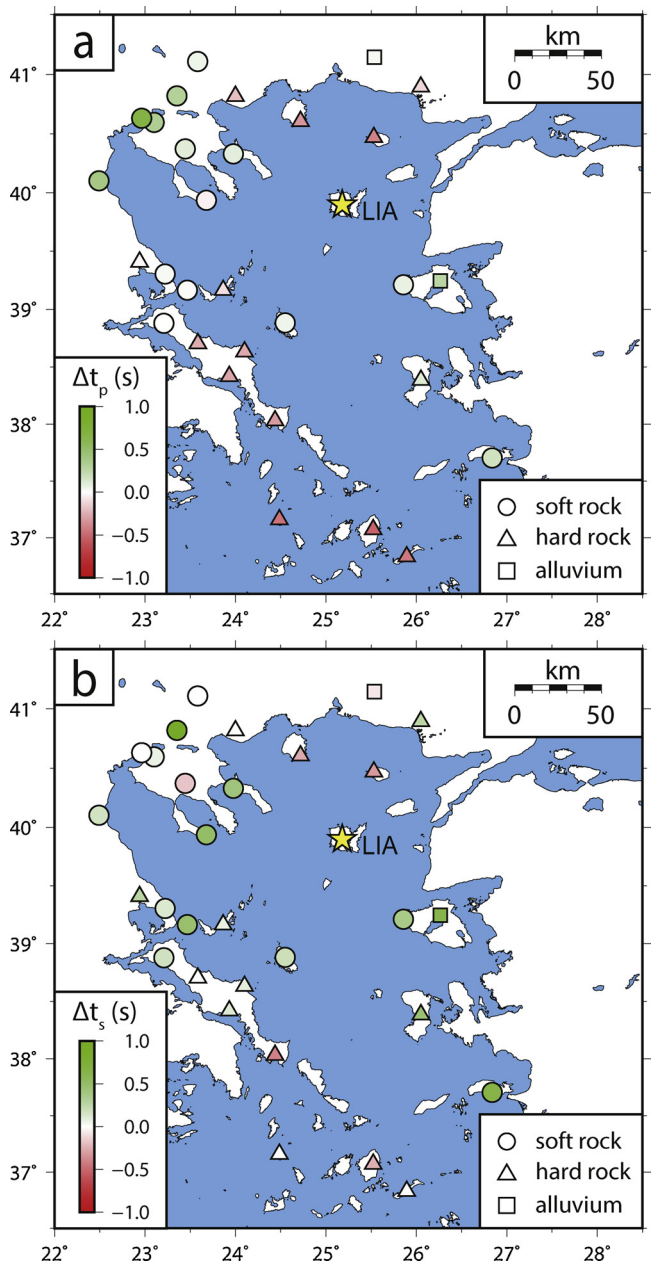

Fig. 5. Maps showing the spatial distribution of inverted station delays in seconds for (a) P-phases, and (b) S-phases. Station symbols indicate the different near-surface geology at the site of each station according to the legend at the lower right hand corner.

occurred during January-March 2017. Clusters of events exhibiting a linear distribution can be seen to extend from the Turkish coast to the south of Agios Efstratios island and to the south of Skyros island. Average horizontal uncertainty was found equal to 3.7 km (± 3 km) while the average vertical uncertainty is 4.8 km (± 2.4 km). Uncertainties increase significantly at longitudes east of 26.5° (i.e. Karaburun peninsula) that are areas outside HUSN, where the closest station is located 50 km away (cf. Fig. 1).

It is interesting to compare the probabilistic nonlinear locations with the routine ones of the NOA catalog in order to assess their differences. In terms of the RMS residual, the use of NLLOC and the minimum 1D model has decreased the average value from 0.38 s in NOA locations to 0.30 s, which implies a reduction of about 21%. The distribution of the RMS residuals for the two kinds of locations appears similar in shape, with a heavier tail at larger values for the distribution

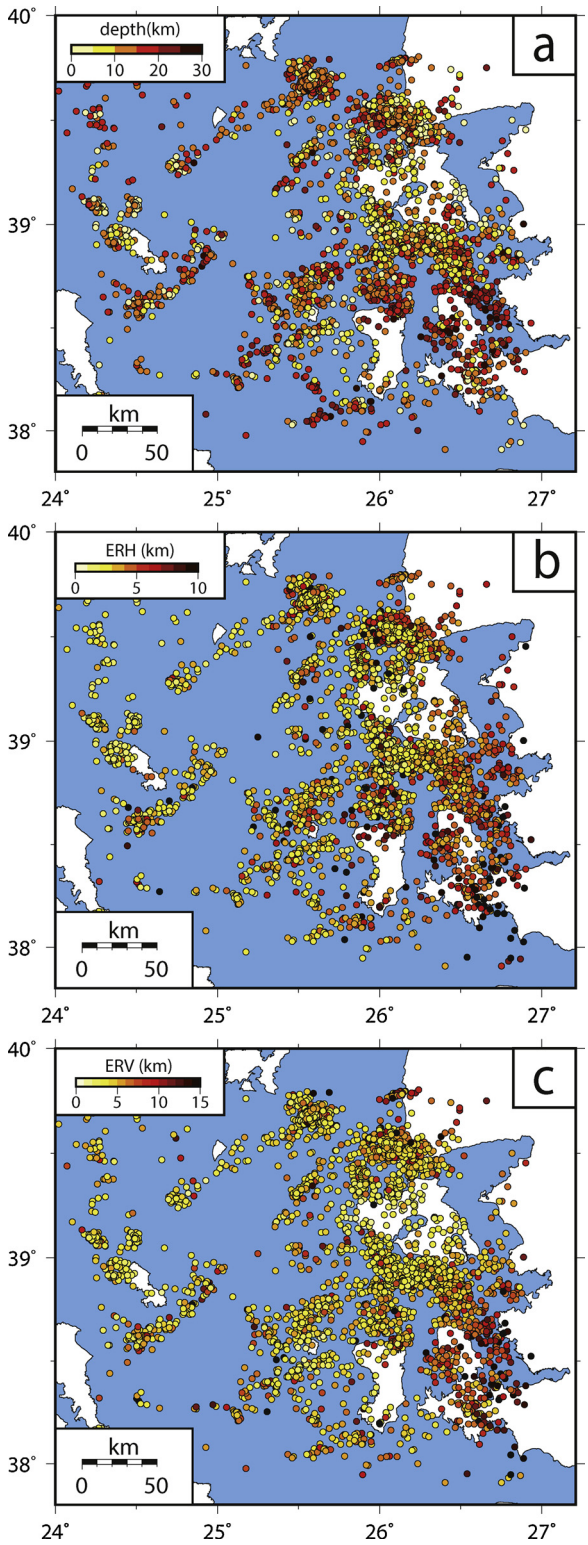

Fig. 6. Maps of NLLOC earthquake locations as a function of (a) hypocentral depth, (b) horizontal error ERH, and (c) vertical error ERV. Note that the extent of the map is larger than that of the red dashed line that outlines the study area in Fig. 1. (For interpretation of the references to colour in this figure legend, the reader is referred to the web version of this article).

of the NOA locations (Fig. 7a). Epicentral locations were found to agree quite well with differences of less than 1 km in most cases; however, this is not the case for hypocentral depths. As can be seen in Fig. 7b, the depth distribution of NLLOC locations shows that the majority of events

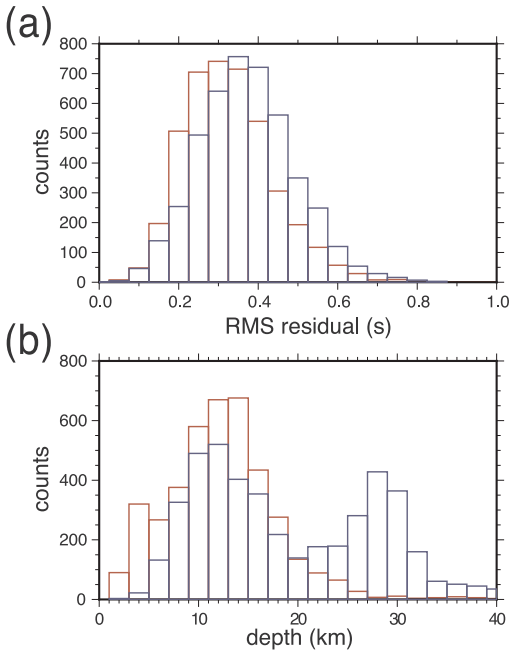

Fig. 7. (a) Comparison between the distribution of RMS residual of NOA routine locations (blue bars) and NLLOC locations (red bars) obtained in this study, (b) the same for hypocentral depths. (For interpretation of the references to colour in this figure legend, the reader is referred to the web version of this article).

nucleated at the top 15 km of the crust and that after this the number of events decreases sharply. This is consistent with the crustal thickness of 25–28 km in the Aegean area (Sodoudi et al., 2006) and a rheology compatible with a brittle upper crust on top of a progressively more ductile lower crust (Konstantinou, 2010). On the other hand, the depth distribution of NOA locations mirrors the NLLOC depth distribution up to about 20 km; instead of decreasing in numbers however, a new peak appears at 28 km and more events are contained at bins deeper than 30 km. This bimodal depth distribution in NOA locations has been also found in a recent study of the seismicity along the North Aegean Trough (Konstantinou, 2017). Synthetic location tests performed in that study had shown that abnormally deep hypocenters may be the result of the relatively simple velocity model used by NOA staff for the location process. The rather low RMS residuals of NOA locations also point to the possibility that stations with large residuals are probably down-weighted by NOA staff in an effort to obtain better location statistics, resulting to a systematic overestimation of the hypocentral depth.

5. Relative locations

5.1. Method

Earthquake locations can be further improved with the calculation of precise relative locations using the double-difference algorithm (also known as HYPODD) developed by Waldhauser and Ellsworth (2000). The algorithm utilizes differential travel times calculated either from catalog data or/and cross-correlation of waveforms in order to minimize the time residual of pairs of events by adjusting the difference in their hypocentral distance. In this study, the requirements for calculating differential travel times involved a separation distance of 10 km for source-receiver distances up to 400 km and that each event connected with 10 other of its neighbors. Following the suggestion of Waldhauser (2001), at least 8 phase pairs are needed in order to consider that neighboring events are strongly linked. From the initial 4,450 events a total of 4,187 were finally selected forming a network of links with 450,015 P-phase and 224,499 S-phase pairs. Most of the events

that were rejected actually fall east of longitude 26.5°, where uncertainties in absolute locations were found to be more than 5 km. The number of average links per event pair was 10 having an average offset between linked events of 4.4 km, while only a small percentage (~2%) of outliers was found. HYPODD uses a 1D P-wave velocity model and a constant Vp/Vs ratio in order to calculate theoretical differential travel times for the P and S phases. For the purposes of this study the P-wave minimum 1D model along with a Vp/Vs ratio of 1.73 were utilized in the relocation. Due to the large number of events the relocation problem was solved by using the LSQR method of damped least-squares. The damping factor was set to 60 by applying the rule of thumb that condition numbers should be between 40–80 for most of the event clusters (Waldhauser, 2001). As in previous HYPODD relocations with HUSN data (e.g. Roumelioti et al., 2003; Konstantinou, 2017) the a priori weights were set to 1.0 for P-phases and 0.5 for S-phases; reweighting was allowed after the first 6 iterations by placing more weight on small inter-event distances. In this way, 3,354 events were finally relocated that represent about 80% of the initially selected events. The average RMS residual dropped after the relocation to 0.06 s (± 0.08 s) that represents a significant reduction compared to the average RMS residual of NLLOC (~0.30 s) and NOA (~0.38 s) locations. Uncertainties of the relocated events were assessed by relocating smaller clusters using the Singular Value Decomposition (SVD) method. Relative horizontal uncertainties reach a value of up to 1.2 km, while the relative vertical ones do not exceed 0.8 km as summarized in Table 2. In what follows, the relocation results are combined with routine focal mechanism solutions provided by NOA and other agencies in order to jointly interpret fault geometry and kinematics.

5.2. Results

5.2.1. Offshore southern Lesvos

The relocated seismicity in the area between Lesvos and Chios islands is dominated by the 12 June 2017 (Mw ~6.3) earthquake and its aftershocks (Fig. 8). Expansion of the aftershock area resulted in a zone with a length of about 40 km by the end of December 2017, which is almost double of what would be expected for an earthquake of this magnitude. The mainshock was relocated to the SE of Lesvos (at 38.8695°, 26.3497°) at a hypocentral depth of 12.6 km and exhibited a purely normal faulting mechanism. The depth cross-section at the SE part of the aftershock zone (cf. Fig. 8 section BB') reveals a tight cluster of events that dips towards SW at an angle of 50°. The depth cross-section at the NW part of the rupture (cf. Fig. 8 section CC') shows a cluster of aftershocks that covers the same depth range, but spreads over a larger area and dips towards SW at a smaller angle (~40°). Some of these aftershocks occur at a distance of 5–10 km from the inferred fault plane, most likely signifying off-fault seismicity. Along the direction of the rupture (cf. Fig. 8 section AA') the depth cross-section shows that aftershocks are distributed from a depth of 15 km to as shallow as 5 km. Recently, Kiratzi (2018) published a slip model of the 12 June mainshock derived from the inversion of weak- and strong-motion data. The main slip patch of this model is superimposed on the relocated aftershocks, where it can be seen that the region of highest slip (90–100 cm) coincides with an area free of any aftershocks. The focal mechanisms of the largest aftershocks as reported by NOA indicate a mixture of normal and strike-slip solutions. At the SE part of the rupture zone normal faulting similar to the mainshock seems to dominate, while solutions with larger components of strike-slip motion appear at the NW part. In the years prior to 2017 the seismicity appears to be concentrated at depths 10–20 km, clustering at the root of the normal fault that ruptured. A similar observation can be inferred for the events that form clusters at the north coast of Chios island and almost all of them occurred in the years before 2017. This concentration of microseismicity at this depth range can be interpreted as an indication that the crust there is strong and capable of nucleating larger events such as the Lesvos earthquake.

Table 2
Details of the clusters relocated using SVD in order to assess relocation relative uncertainties. Neq is the number of earthquakes contained in each cluster, cLat cLon cH represent the cluster centroid location and depth, and ErrX ErrY ErrZ are the corresponding mean uncertainties.

ID	Neq	cLat	clon	cH (km)	ErrX (km)	ErrY (km)	ErrY (km)
1	62	39.411	25.93	6.59	1	1.2	0.8
2	43	38.696	25.499	13.55	0.31	0.26	0.55
6	20	38.844	25.993	14.93	0.13	0.05	0.13
4	55	38.615	24.526	13.74	0.48	0.61	0.57
5	51	38.6	24.525	13.15	0.55	0.5	0.62
6	12	39.809	26.101	16.95	0.09	0.03	0.11

5.2.2. Biga peninsula-northern Lesvos

The seismic activity at Biga peninsula started in early January 2017 with small magnitude (M_L < 3.0) earthquakes that culminated in the generation of four moderate magnitude (Mw ~5.0–5.2) events in February 2017. Two of these events occurred on 6 February (at 03:51:41 and 10:58:02 UTM respectively), the third one occurred the next day (07/02) and the fourth on 12 February. The activity continued with numerous smaller earthquakes throughout March and started declining from early April, however, events continued to occur sporadically until December 2017. Reported focal mechanisms indicate pure normal faulting along NW-SE direction. Fig. 9 shows the relocated seismicity at Biga peninsula and offshore northern Lesvos where it can be seen that the epicentral locations indeed form a NW-SE cluster that covers the tip of the peninsula and extends offshore towards NW. The seismicity looks more scattered in the area between the Turkish coast and the northern coast of Lesvos without exhibiting any clear correlation with known faults. The two perpendicular depth cross-sections give a sharp image of the fault geometry, depicting a curved listric fault that dips towards SW, extending from a depth of about 3 km down to 17 km. Cross-section BB' also reveals that an antithetic fault, dipping towards NE, was activated almost at the same time even though it only generated small magnitude events. The first three moderate magnitude events are well-aligned along the curved surface of the fault, with the first (06/02 at 03:51) nucleating at a depth of 12 km, the second (06/02 at 10:58) at 14 km and the third (07/02) at 16 km. This spatio-temporal sequence implies that the rupture propagated progressively downwards within a period of 2 days. The dipping of the fault planes support this spatio-temporal relationship, since the dip angle changed from 50° for the first event to 38° for the second and 34° for the third and deepest event. The fourth event (12/02) is located further to the east at a depth of 6 km and is probably the result of stresses within the shallow crust induced by the three earlier events. It should be noted that the steep shallow part of the activated listric fault and its antithetic agree with field observations that show high-angle normal faulting being a major seismotectonic feature in the Biga peninsula (Sözbilir et al., 2016). Depth cross-section AA' along the ruptured surface shows two large clusters of events that combine to define a fault with a total length of 17 km. Seismicity that occurred prior to 2017 appears to be evenly distributed among different depths as shown in the depth cross-sections and seems to envelope the area that ruptured during the swarm. The downward propagation of the rupture, coupled with the fact that the location of the swarm coincides spatially with the actively exploited Tuzla geothermal field, put forward the suggestion that the swarm may represent an example of induced seismicity.

5.2.3. Skyros-Edremit zone

The line that connects Edremit Gulf with the island of Skyros coincides with the orientation of the different branches of the North Anatolian Fault within the Aegean. Indeed, the relocated seismicity along this line exhibits elongated clusters that mostly coincide with strike-slip faults that exist in this area (Fig. 10). The majority of these

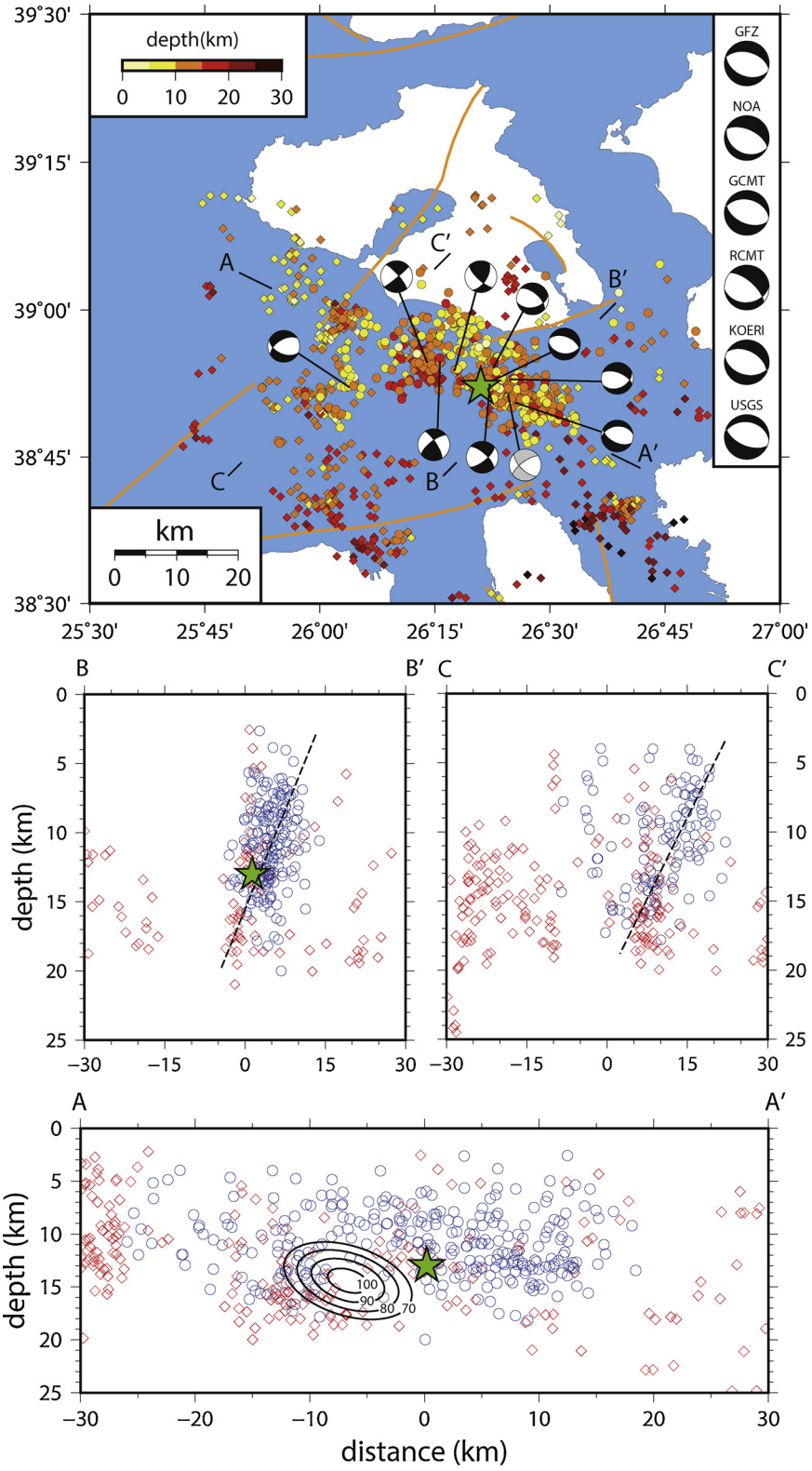

Fig. 8. Upper panel: Map showing the distribution of relative locations for the area of southern Lesvos-northern Chios. The green star indicates the location of the 12 June 2017 Lesvos earthquake. Circles correspond to aftershocks while diamonds represent events that occurred prior to the Lesvos earthquake. Beach balls represent focal mechanism solutions of aftershocks taken from the moment tensor database of NOA, Institute of Geodynamics. The grey beach ball indicates the focal mechanism solution for the largest aftershock. The panel at the right hand side lists the focal mechanism solutions of the mainshock that were reported by various groups/agencies. Lower panel: Depth cross-sections corresponding to the profiles shown on the map. Blue circles are aftershocks while red diamonds are events prior to the 12 June 2017 earthquake. Dashed black lines outline the orientation of inferred fault planes. Solid black ellipses represent slip contours of the patch that ruptured during the mainshock obtained from the study of Kiratzi (2018). (For interpretation of the references to colour in this figure legend, the reader is referred to the web version of this article).

events have local magnitudes smaller than 3.5 and only two events, one on 8 January 2013 and another on 11 October 2017 have larger magnitudes. The former event was the largest (Mw ~5.6) and was located at the edge of the fault that produced the 1968 Agios Efstratios earthquake. It was followed by numerous aftershocks distributed along the fault plane as well as along parallel strands (for details see Karakostas et al., 2014; Ganas et al., 2014). The latter event was a moderate one (Mw ~5.0) located at the NW of Skyros and it nucleated along the same fault that produced the 2001 strong earthquake (cf. Table 1 and Fig. 1). Depth cross-section AA' covers the area along Skyros island where it can be seen that the majority of the relocated earthquakes occur at the edges of the main slip patch of the 2001 earthquake (cf. Fig. 10). The other depth cross-section (BB') runs along the main NE-SW branch of the North Anatolian Fault, part of which ruptured on 19 December

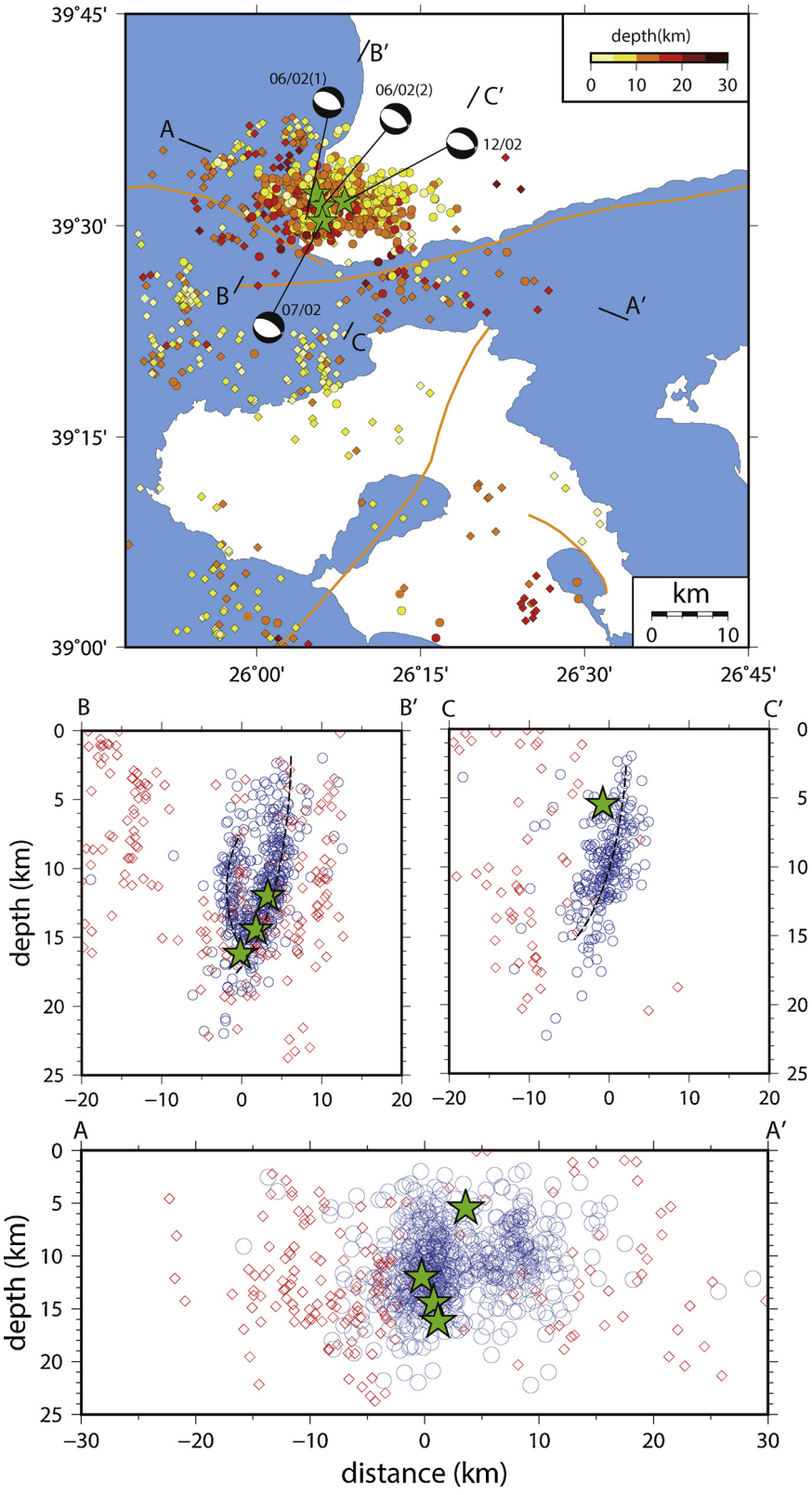

Fig. 9. Upper panel: Map showing the distribution of relative locations for the area of Biga peninsula-northern Lesvos. The green stars indicate the locations of the four moderate events that occurred in January-February 2017. Circles correspond to events of the January-March 2017 swarm, while diamonds are events that occurred prior to 2017. Beach balls represent focal mechanism solutions of aftershocks taken from the moment tensor database of NOA, Institute of Geodynamics. Lower panel: Depth cross-sections corresponding to the profiles shown on the map. Blue circles are hypocenters of swarm events and red diamonds are hypocenters of events that occurred prior to 2017. (For interpretation of the references to colour in this figure legend, the reader is referred to the web version of this article).

1981 during a strong (Mw ~6.8) earthquake (cf. Table 1 and Fig. 1). The seismicity defines linear features at the SW and at the NE part of this fault, effectively encompassing the segment that ruptured in 1981. This segment seems to be devoid of any earthquakes and has a length of about 43 km (cf. Fig. 10). Other smaller clusters appear to the north and south of the island of Psara and coincide with known active faults. The available focal mechanisms confirm the dominance of strike-slip faulting in the area (along NE-SW or NW-SE directions), but normal faulting events along the WNW-ESE direction are also present.

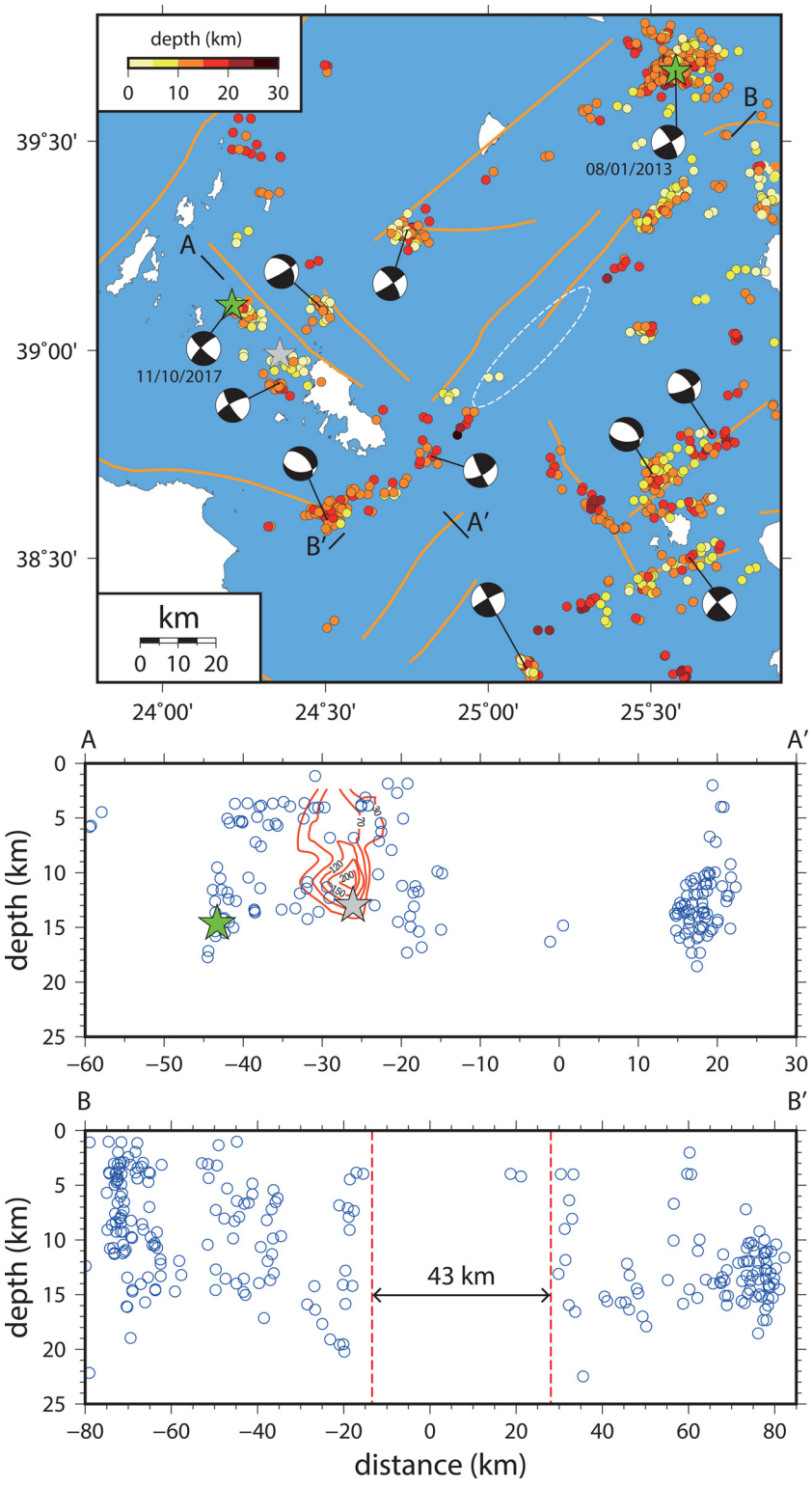

Fig. 10. Upper panel: Map showing the distribution of relative locations for the area of the Skyros-Edremit zone. The green stars indicate the locations of events with magnitude larger than 5.0, while the gray star signifies the location of the 2001 Skyros earthquake. The dashed-line ellipse delineates the rupture zone of the 19 December 1981 event. Beach balls represent focal mechanism solutions taken from the moment tensor database of NOA, Institute of Geodynamics. Lower panel: Depth cross-sections corresponding to the profiles shown on the map. The solid red curves in section AA' correspond to contours of slip (in cm) for the 2001 Skyros earthquake obtained from Roumelioti et al. (2004). Red dashed lines in section BB' delineate the part that corresponds to the rupture zone of the 19 December 1981 earthquake. (For interpretation of the references to colour in this figure legend, the reader is referred to the web version of this article).

6. Discussion

6.1. Seismicity and regional stress

The precise location of seismicity in NE Aegean offers the opportunity to compare it with known active faults and also to examine its relationship with the regional stress field. Fig. 11 shows the traces of active faults included in the GReDaSS database (Caputo and Pavlides, 2013) and their sense of motion based on kinematic indicators such as focal mechanisms. The Figure also includes faults that were found to be seismically active during the period of this study but are not included in GReDaSS. The present-day stress field in the Aegean and mainland Greece has been recently derived by Konstantinou et al. (2016) after a damped inversion of a large number of focal mechanisms along a regular grid with a node spacing of 0.35°. A significant property of these stress inversion results is that they only contain the degree of spatial variation that is strongly required by the data. The orientations of the minimum stress axes for each node are superimposed on the other

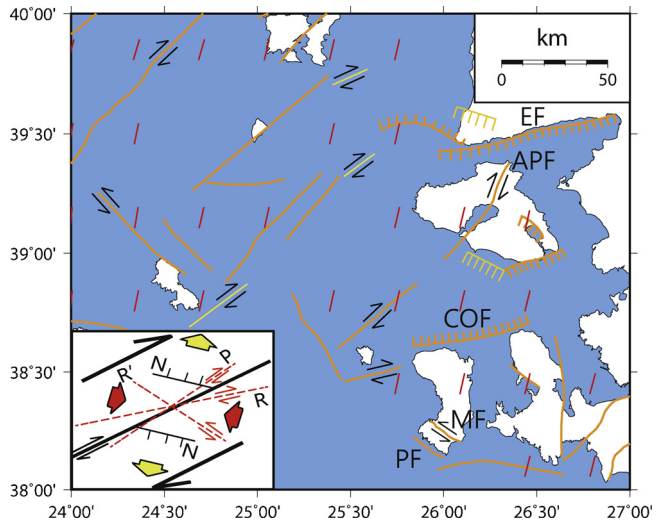

Fig. 11. Map depicting the main tectonic elements in the area of NE Aegean. Orange lines are active faults included in the GReDaSS database, while yellow lines are faults that exhibited seismic activity during 2011–2017. Thin red bars symbolize the orientation of minimum stress axes derived by Konstantinou et al. (2016). Black arrows give a sense of motion for strike-slip faults and comb-like lines correspond to normal faults. EF: Edremit Fault, APF: Agia Paraskevi Fault, COF: Chios-Oinnouses Fault, MF: Mastichochoria Fault, PF: Philadelphia Fault. The inset at the lower left hand corner explains the geometry and kinematics of strike-slip and normal faults in relation to extensional and compressional directions. (For interpretation of the references to colour in this figure legend, the reader is referred to the web version of this article).

features in Fig. 11, while their plunge angle ranges between 5°–10°. Uncertainties in both orientation and plunge angle of the stress axes did not exceed 10° and were inferred by using a bootstrap resampling technique. The dominant structural feature in Fig. 11 is the parallel strands of dextral strike-slip faults that accommodate the westward motion of the Anatolian plate. These strands essentially represent principal shear zones that form obliquely to the minimum stress axes, followed occasionally by P or R Riedel shears. The NW-SE strike-slip faults with sinistral motion are intersected by the minimum stress axes at a high angle and therefore may correspond to R' Riedel shears. Normal faults can form with a strike nearly perpendicular to the minimum stress axes, as exemplified by the 12 June 2017 Lesvos earthquake and the Biga peninsula events. Such a transtentional deformation pattern can be attributed to the combined effect of the Anatolian westward push and the gravitational spreading of the Aegean plate caused by slab rollback along the Hellenic subduction zone (Meijer and Wortel, 1997; Konstantinou et al., 2016).

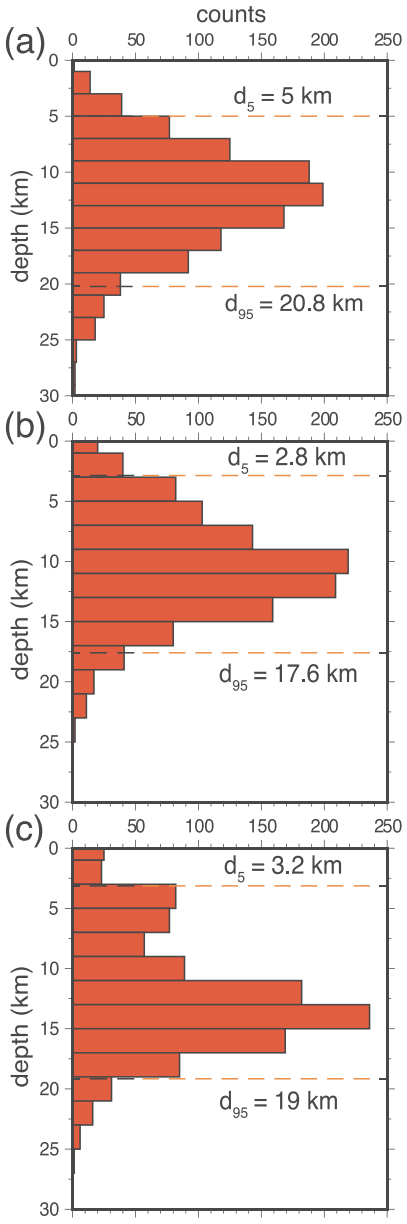

Fig. 12. Histograms that show the distribution of relocated hypocentral depth in (a) southern Lesvos-northern Chios, (b) Biga peninsula-northern Lesvos, and (c) Skyros-Edremit zone. Symbols d5 and d95 represent the 5th and 95th percentile of the depth in each distribution.

6.2. Implications for seismic hazard

The hypocenters derived in this study can also be utilized for inferring the seismogenic layer thickness, which is an important parameter for estimating expected earthquake magnitudes along specific faults. As noted previously by Wyss (1979), fault length alone cannot provide accurate estimates of expected magnitude for the reason that the amount of elastic energy released during an earthquake also depends on the fault width. In this sense, scaling relationships that connect moment magnitude **M** with rupture area A are the most appropriate for evaluating the seismogenic potential of faults in NE Aegean. Konstantinou (2014) developed such relationships for earthquakes in the Mediterranean region and found that when $A > 251\,km^2$ the moment magnitude is given by

$$\mathbf{M} = (4/3)\log A + 3.07$$

Using the value of seismogenic layer thickness H it is possible to estimate the fault width as $W = H/\sin\delta$ where δ is the dip of the particular fault and A is then equal to the product L × W, where L is the length of the fault. Fig. 12 shows the depth distribution for the Lesvos-Chios, Biga peninsula and Skyros-Edremit zone that contain the bulk of the relocated events. The onset and cutoff depths of the seismicity are calculated for each distribution as the 5th and 95th percentile, respectively. The difference of these two values is taken as the seismogenic layer thickness H, which seems to be very similar in all three areas (14.8–15.8 km). As an example of this procedure, it is possible to estimate the moment magnitude of the 19 December 1981 earthquake mentioned earlier. For this fault L = 43 km and W = 15.8/sin(90°) yielding a rupture area $A = 679\ km^2$. It can be easily verified that **M** = 6.8 which is consistent with the moment magnitude reported in the ISC-GEM catalog (Storchak et al., 2013). Using the 10th and 90th percentile as onset/cutoff depths for the estimation of H would only slightly change the magnitude value (**M** = 6.7). On the other hand, an overestimation would occur in the case when the 1st and 99th

Table 3
Summary of the geometrical properties of active faults in the study area that may produce strong earthquakes. L is the fault length, δ is the dipping angle, W is the fault width, A is the rupture area, **M** is the calculated expected moment magnitude and T is the period since the last major earthquake. APF: Agia Paraskevi Fault, EF: Edremit Fault, COF: Chios-Oinnouses Fault, MF: Mastichochoria Fault, PF: Philadelphia Fault (see text and also map in Fig. 11).

Fault	L (km)	δ	W (km)	A (km^2)	M	T (years)
APF (onshore)	20	90°	15.8	316	6.4	151
APF (offshore)	32	90°	15.8	505	6.7	151
APF (both)	52	90°	15.8	821	6.9	151
EF	75	63°	16.6	1245	7.2	74
COF (scenario 1)	30	60°	18.2	546	6.7	69
COF (scenario 2)	58	60°	18.2	1055	7.1	69
MF	20	87°	15.8	316	6.4	137(*)
PF	17	80	16	272	6.3	137(*)

Scenario 1: only the segment parallel to the northern coast of Chios ruptures. Scenario 2: the rupture also extends to the Turkish coast. (*) These are the two candidate faults responsible for the 3 April 1881 Chios-Cesme event.

percentiles were used, yielding H = 22.2 km and **M** = 7.0.

There are four faults within the study area that can be considered as the most likely sites for future strong earthquakes, these are namely the Agia Paraskevi Fault (APF) in Lesvos island, the Edremit Fault (EF) along the southern coast of the Biga peninsula, the Chios-Oinnouses (COF) and Mastichohoria Fault (MF) in Chios island (cf. Fig. 11). All four of these faults have produced in the past strong earthquakes with magnitudes larger than 6.0, while the time period since the last earthquake varies among them between 69 and 151 years. Geometrical characteristics of these faults are known from published studies such as Chatzipetros et al. (2013) for APF, COF, MF and Sözbilir et al. (2016) for EF. When estimating expected magnitudes for APF and COF different rupture lengths are considered in order to take into account the uncertainties in their total length. Table 3 gives a summary of these fault characteristics as well as the expected magnitude in each case. Despite the fact that EF and COF are capable of producing large earthquakes with magnitudes from 6.7 to 7.2, the period since the last strong event in either fault is likely too short (69–74 years) for allowing the nucleation of another major earthquake within the next few years. On the contrary, APF and MF have both been seismically silent for over 100 years, therefore the discussion that follows will focus on these two faults.

APF is a strike-slip fault thought to be responsible for a strong earthquake on 7 March 1867 that caused 550 casualties in Lesvos island and the neighboring Turkish coast. Macroseismic as well as geochemical observations constrain the trace of the rupture on land (Fytikas et al., 1999; Papazachos and Papazachou, 2003); however, its continuation offshore within the Kalloni Gulf is a matter of debate. Roumelioti and Kiratzi (2010) simulated strong ground motion acceleration for the 1867 event by considering the same rupture lengths as the ones shown in Table 3. They concluded that intensities, inferred from simulated peak ground acceleration values, were similar to macroseismic intensities only when the fault length did not exceed 20 km (Mw ~6.4), favoring a rupture that extends only onshore. The first scenario therefore considers that only the onshore segment of the fault ruptures; a second scenario assumes that the segment that ruptures includes the whole length of the Kalloni Gulf; and the third one deals with the rupture of both onshore and offshore segments. Expected moment magnitudes for these scenarios range from 6.4 to 6.9. On the other hand, MF is a strike-slip fault that is likely related to the 3 April 1881 Chios-Cesme earthquake which was the deadliest event to strike this area with more than 3500 casualties (Papazachos and Papazachou, 2003; Altinok et al., 2005). Assuming a rupture along its total length, the expected moment magnitude is 6.4, a value which agrees well with the magnitude of the 1881 event proposed by Papazachos and Papazachou (2003). At this point it should be mentioned that Chatzipetros et al. (2013) suggest that another fault, the Philadelphia Fault (PF) may also be a candidate source for the 1881 earthquake. The trace of this fault is parallel to the south coast of Chios island (cf. Fig. 11) and it may correspond to a normal fault based on a steep scarp seen in the shoreline morphology. The expected magnitude of a potential earthquake along PF is 6.3, only slightly lower than MF.

A general observation is that very few earthquakes were located during the study period along APF and almost none along MF (cf. Figs. 6, 8 and 9). This cannot be attributed to the completeness of the NOA catalog, since it has been found that seismicity recorded by HUSN in NE Aegean is complete down to magnitude 2.0 (D'Alessandro et al., 2011). Lack of seismicity may hence signify either that these faults are experiencing aseismic creep, or that they are locked and thus accumulate strain energy. Indeed, this is in accordance with the observation that in the Aegean area geodetic strain rates constrained by GPS data, are higher than the seismic ones calculated by using historical earthquake catalogs (see for example Rontogianni, 2010). Considering the seismogenic potential of these faults and that they traverse densely populated areas, it is of crucial importance that both of them are closely monitored so as to understand their deformation behavior.

7. Conclusions

This study utilized the recorded seismicity in the NE Aegean during 2011–2017 in order to derive a minimum 1D velocity model with station delays and to obtain precise relative locations that delineate active faults in the area. The main conclusions of this work can be summarized as follows:

1 Improved absolute locations of 4450 events were obtained using the nonlinear probabilistic algorithm NLLOC and the newly derived velocity model with station delays. Estimated uncertainties were found to be less than 5 km both horizontally and vertically, however, east of longitude 26.5° these uncertainties increase significantly. A comparison of these improved locations with the routine ones provided by NOA showed differences in hypocentral depth distribution that are most likely caused by the simplified velocity model used in routine analysis and down-weighting of stations with large RMS residuals.
2 Precise relative locations of 3354 events were obtained by using the double-difference algorithm HYPODD, resulting in location uncertainties of 1.2 km or less both horizontally and vertically. The relocated seismicity delineates the normal fault that produced the 12 June 2017 Lesvos earthquake and also the listric fault that was activated during the January-March 2017 earthquake sequence at Biga peninsula. Linear strands of strike-slip faults along the Skyros-Edremit zone were also delineated, as well as a 43 km segment that is devoid of any earthquakes and corresponds to the rupture zone of the 19 December 1981 (Mw ~6.8) earthquake in the central Aegean.
3 The seismotectonic pattern in this area can be explained in terms of transtensional deformation as a result of the combined westward push of the Anatolia plate and the gravitational spreading of the Aegean lithosphere. This leads to the development of principal shear zones along with P, R, R' Riedel shears and normal faulting perpendicular to the direction of the minimum stress axes.
4 The seismogenic layer thickness in NE Aegean, expressed as the difference between the 5th and 95th percentile of the hypocentral depth distribution, is between 14.8–15.8 km. Based on these values and geometrical characteristics of faults in the area, the expected moment magnitude of potential earthquakes is estimated in the range of 6.4–7.2 depending on the choice of rupture scenario. Of particular concern are the faults of Agia Paraskevi in Lesvos and Mastichochoria in Chios that are thought to be responsible for strong earthquakes in 1867 and 1881 respectively. These two faults appear almost aseismic, an observation that can be interpreted either as a

sign of creeping, or as a sign that they are locked and accumulate strain energy. Continuous seismic and geodetic monitoring is needed in order to investigate which of these two interpretations is valid.

Acknowledgments

I would like to thank the Ministry of Science and Technology of Taiwan (MOST) for the financial support of this study in the form of an awarded grant. I am grateful to the staff of the National Observatory of Athens, Institute of Geodynamics, for data archiving/processing and to Wen-Tzong Liang for computational support. I would also like to thank two anonymous reviewers for their helpful comments and the Editor-in-Chief, Irina Artemieva for handling the manuscript. The catalog of relocated events is available from the author upon request.

References

Akyol, N., Zhu, L., Mitchell, B.J., Sözbilir, H., Kekovali, K., 2006. Crustal structure and local seismicity in western Anatolia. Geophys. J. Int. 166, 1259–1269. https://doi.org/10.1111/j.1365-246X.2006.03053.x.

Altinok, Y., Alpar, B., Özer, N., Gazioglou, C., 2005. 1881 and 1949 earthquakes at the Chios-Cesme Strait (Aegean Sea) and their relation to tsunamis. Nat. Hazard Earth Syst. Sci. 5, 717–725.

Beniest, A., Brun, J.P., Gorini, C., Grombez, V., Deschamps, R., Hamon, Y., Smit, J., 2016. Interaction between trench retreat and Anatolian escape as recorded by neogene basins in the northern Aegean Sea. Mar. Petroleum Geol. 77, 30–42. https://doi.org/10.1016/j.marpetgeo.2016.05.011.

Caputo, R., Pavlides, S., 2013. The Greek Database of Seismogenic Sources (GreDaSS), Version 2.0.0: a Compilation of Potential Seismogenic Sources (Mw & 5.5) in the Aegean Region. https://doi.org/10.15160/unife/gredass/0200. http://gredass.unife.it/.

Chatzipetros, A., Kiratzi, A., Zouros, N., Pavlides, S., 2013. Active faulting in the north-eastern Aegean sea islands. Tectonophysics 597-598, 106–122. https://doi.org/10.0116/j.tecto.2012.11.026.

D'Alessandro, A., Papanastassiou, D., Baskoutas, I., 2011. Hellenic unified seismic network: an evaluation of its performance through SNES method. Geophys. J. Int. 185, 1417–1430. https://doi.org/10.1111/j.1365-246X.2011.05018.x.

Floyd, M.A., Billiris, H., Paradisis, D., Veis, G., Avallone, A., Briole, P., McClusky, S., Nocquet, J.-M., Palamartchouk, K., Parsons, B., England, P.C., 2010. A new velocity field for Greece: implications for the kinematics and dynamics of the Aegean. J. Geophys. Res. 115, B10403. https://doi.org/10.1029/2009JB007040.

Font, Y., Kao, H., Lallemand, S., Liu, C.S., Chiao, L.Y., 2004. Hypocenter determination offshore of eastern Taiwan using the maximum intersection method. Geophys. J. Int. 158, 655–675.

Fytikas, M., Lombardi, S., Papachristou, M., Pavlides, S., Zouros, N., Soulakelis, N., 1999. Investigation of the 1867 Lesbos (NE Aegean) earthquake fault pattern based on soil-gas geochemical data. Tectonophysics 308, 249–261.

Ganas, A., Roumelioti, Z., Karastathis, V., Chousianitis, K., Moshou, A., Mouzakiotis, E., 2014. The Lemnos 8 January 2013 (Mw = 5.7) earthquake: fault slip, aftershock properties and static stress transfer modeling in the north Aegean Sea. J. Seismol. 18, 433–455. https://doi.org/10.1007/s10950-014-9418-3.

Hatzfeld, D., Martinod, J., Bastet, G., Gautier, P., 1997. An analog experiment for the Aegean to describe the contribution of gravitational potential energy. J. Geophys. Res. 102, 649–659.

Hollenstein, C., Müller, M.D., Geiger, A., Kahle, H.-G., 2008. Crustal motion and deformation in Greece from a decade of GPS measurements, 1993-2003. Tectonophysics 449. https://doi.org/10.1016/j.tecto.2007.12.006.

Karagianni, E., Papazachos, C.B., Panagiotopoulos, D.G., Suhaldoc, P., Vuan, A., Panza, G.F., 2005. Shear velocity structure in the Aegean area obtained by inversion of Rayleigh waves. Geophys. J. Int. 160, 127–143. https://doi.org/10.1111/j.1365-246X.2005.02354.x.

Karakostas, V., Papadimitriou, E.E., Karakaisis, G.F., Papazachos, C.B., Scordilis, E.M., Vargemezis, G., Aidona, E., 2003. The 2001 Skyros, Northern Aegean, Greece, earthquake sequence: off-fault aftershocks, tectonic implications, and seismicity triggering. Geophys. Res. Lett. 30, 1012. https://doi.org/10.1029/2002GL015814.

Karakostas, V., Papadimitriou, E., Gospondinov, D., 2014. Modeling the 2013 North Aegean (Greece) seismic sequence: geometrical and frictional constraints, and aftershock probabilities. Geophys. J. Int. 197, 525–541. https://doi.org/10.1093/gji/ggt523.

Kiratzi, A., 2002. Stress tensor inversions along the westernmost North Anatolian Fault Zone and its continuation into the North Aegean Sea. Geophys. J. Int. 151, 360–376.

Kiratzi, A., 2018. The 12 June 2017 Mw 6.3 Lesvos island (Aegean Sea) earthquake: slip model and directivity estimated with finite-fault inversion. Tectonophysics 724-725, 1–10. https://doi.org/10.1016/j.tecto.2018.01.003.

Kissling, E., 1995. Program VELEST User's Guide - Short Introduction, Institute of Geophysics. ETH Zurich.

Kissling, E., Ellsworth, W.L., Eberhart-Phillips, D., Kradolfer, U., 1994. Initial reference models in local earthquake tomography. J. Geophys. Res. 99, 19635–19646.

Konstantinou, K.I., 2010. Crustal rheology of the Santorini-Amorgos zone: implications for the nucleation depth and rupture extent of the 9 July 1956 Amorgos earthquake, southern Aegean. J. Geodyn. 50, 400–409. https://doi.org/10.1016/j.jog.2010.05.002.

Konstantinou, K.I., 2014. Moment magnitude-rupture area scaling and stress-drop variations for earthquakes in the Mediterranean region. Bull. Seismol. Soc. Am. 104, 2378–2386. https://doi.org/10.1785/0120140062.

Konstantinou, K.I., 2017. Accurate relocation of seismicity along the North Aegean Trough and its relation to active tectonics. Tectonophysics 717, 372–382. https://doi.org/10.1016/j.tect.2017.08.021.

Konstantinou, K.I., Mouslopoulou, V., Liang, W.-T., Heidbach, O., Oncken, O., Suppe, J., 2016. Present-day crustal stress field in Greece inferred from regional-scale damped inversion of earthquake focal mechanisms. J. Geophys. Res. Solid Earth 121. https://doi.org/10.1002/2016JB013272.

Koukouvelas, I.K., Aydin, A., 2002. Fault structure and related basins of the North Aegean Sea and its surroundings. Tectonics 21, 1046. https://doi.org/10.1029/2001TC901037.

Kreemer, C., Chamot-Rooke, N., Le Pichon, X., 2004. Constraints on the evolution and vertical coherency of deformation in the Northern Aegean from a comparison of geodetic, geologic and seismologic data. Earth Planet. Sci. Lett. 225, 329–346. https://doi.org/10.1016/j.epsl.2004.06.018.

Lomax, A., Curtis, A., 2001. Fast, probabilistic earthquake location in 3D models using Oct-Tree importance sampling. Geophys. Res. Abstr. 3.

Lomax, A., Virieux, J., Volant, P., Berge-Thierry, C., 2000. Probabilistic earthquake location in 3D and layered models. In: Thurber, Rabinowitz (Ed.), Advances in Seismic Event Location, pp. 101–134.

Lomax, A., Michelini, A., Curtis, A., 2009. Earthquake Location, Direct, Global-Search Methods, in Complexity In Encyclopedia of Complexity and System Science, Part 5. Springer, New York, pp. 2449–2473. https://doi.org/10.1007/978-0-387-30440-3.

Maleki, V., Hossein Shomali, Z., Hatami, M.R., Pakzad, M., Lomax, A., 2013. Earthquake relocation in the central Alborz region of Iran using a nonlinear probabilistic method. J. Seismol. 17, 615–628. https://doi.org/10.1007/s10950-012-9342-3.

McNeill, L.C., Mille, A., Minshull, T.A., Bull, J.M., Kenyon, N.H., 2004. Extension of the North Anatolian Fault into the North Aegean Trough: evidence for transtension, strain partitioning, and analogues for Sea of Marmara basin models. Tectonics 23, TC2016. https://doi.org/10.0129/2002TC001490.

Meijer, P.T., Wortel, M.J.R., 1997. Present-day dynamics of the Aegean region: a model analysis of the horizontal pattern of stress and deformation. Tectonics 16, 879–895.

Moser, T.J., Van Eck, T., Nolet, G., 1992. Hypocenter determination in strongly heterogeneous earth models using the shortest path method. J. Geophys. Res. 97, 6563–6572.

Müller, M.D., Geiger, A., Kahle, H.-G., Veis, G., Billiris, H., Paradissis, D., Felekis, S., 2013. Velocity and deformation fields in the North Aegean domain, Greece, and implications for fault kinematics, derived from GPS data 1993-2009. Tectonophysics 597-598 (34-40). https://doi.org/10.1016/j.tecto.2012.08.003.

Nyst, M., Thatcher, W., 2004. New constraints on the active tectonic deformation of the Aegean. J. Geophys. Res. 109, B11406. https://doi.org/10.1029/2003JB002830.

Papanikolaou, D., Alexandri, M., Nomikou, P., Ballas, D., 2002. Morphotectonic structure of the western part of the North Aegean Basin based on swath bathymetry. Mar. Geol. 190, 465–492.

Papazachos, B.C., Papazachou, K., 2003. The Earthquakes of Greece, Ziti Editions. Thessaloniki. .

Podvin, P., Lecomte, I., 1991. Finite difference computation of traveltimes in very contrasted velocity models: a massively parallel approach and its associated tools. Geophys. J. Int. 105, 271–284.

Reilinger, R., McClusky, S., Paradisis, D., Ergintav, S., Vernant, P., 2010. Geodetic constraints on the tectonic evolution of the Aegean region and strain accumulation along the Hellenic subduction zone. Tectonophysics 488, 22–30. https://doi.org/10.1016/j.tecto.2009.05.027.

Rontogianni, S., 2010. Comparison of geodetic and seismic strain rates in Greece by using a uniform processing approach to campaign GPS measurements over the interval 1994-2000. J. Geodyn. 50, 381–399. https://doi.org/10.1016/j.jog.2010.04.008.

Roumelioti, Z., Kiratzi, A., 2010. Incorporating different source rupture characteristics into simulations of strong ground motion from the 1867 M7.0 earthquake on the island of Lesvos (NE Aegean Sea, Greece). Bull. Geol. Soc. Greece XLIII, 2135–2143.

Roumelioti, Z., Kiratzi, A., Melis, N., 2003. Relocation of the 26 July 2001 Skyros island (Greece) earthquake sequence using the double-difference technique. Phys. Earth Planet. In. 138, 231–239.

Roumelioti, Z., Kiratzi, A., Dreger, D., 2004. The source process of the 2001 July 26 Skyros island (Greece) earthquake. Geophys. J. Int. 156, 541–548. https://doi.org/10.1111/j.1365-246X.2004.02124.x.

Sodoudi, F., Kind, R., Hatzfeld, D., Priestley, K., Hanka, W., Wylegalla, K., Stavrakakis, G., Vafidis, A., Harjes, H.-P., Bohnhoff, M., 2006. Lithospheric structure of the Aegean obtained from P and S receiver functions. J. Geophys. Res. 111, B12307. https://doi.org/10.1029/2005JB003932.

Sözbilir, H., Sümer, Ö., Özkaymak, C., Uzel, B., Güler, T., Eski, S., 2016. Kinematic analysis and palaeoseismology of the Edremit Fault Zone: evidence for the past earthquakes in the southern branch of the North Anatolian Fault Zone, Biga Peninsula, NW Turkey. Geodyn. Acta 28, 273–294. https://doi.org/10.1080/09853111.2016.1175294.

Storchak, D., Di Giacomo, D., Bondár, I., Engdahl, E.R., Harris, J., Lee, W.H.K., Villaseñor, A., Bormann, P., 2013. Public release of the ISC-GEM global instrumental earthquake catalog. Seismol. Res. Lett. 84, 810–815. https://doi.org/10.1785/02.20130034.

Tarantola, A., Valette, B., 1982. Inverse problems = quest for information. J. Geophys. 50, 159–170.

Waldhauser, F., 2001. HypoDD: A Program to Compute Double-difference Hypocentre Locations. U. S. Geological Survey Open File Report 01-113.

Waldhauser, F., Ellsworth, W.L., 2000. A double-difference earthquake location algorithm: method and application to the northern Hayward fault, California. Bull. Seism. Soc. Am. 90 (6), 1353–1368.

Wyss, M., 1979. Estimating maximum expectable magnitude of earthquakes from fault dimensions. Geology 7, 336–340.